Matter, Volume *5*

Supplemental information

Identifying infectiousness of SARS-CoV-2 by ultra-sensitive SnS_2 SERS biosensors with capillary effect

Yusi Peng, Chenglong Lin, Yanyan Li, Yong Gao, Jing Wang, Jun He, Zhengren Huang, Jianjun Liu, Xiaoying Luo, and Yong Yang

Supplemental Information

I-Supplemental Figures and Notes

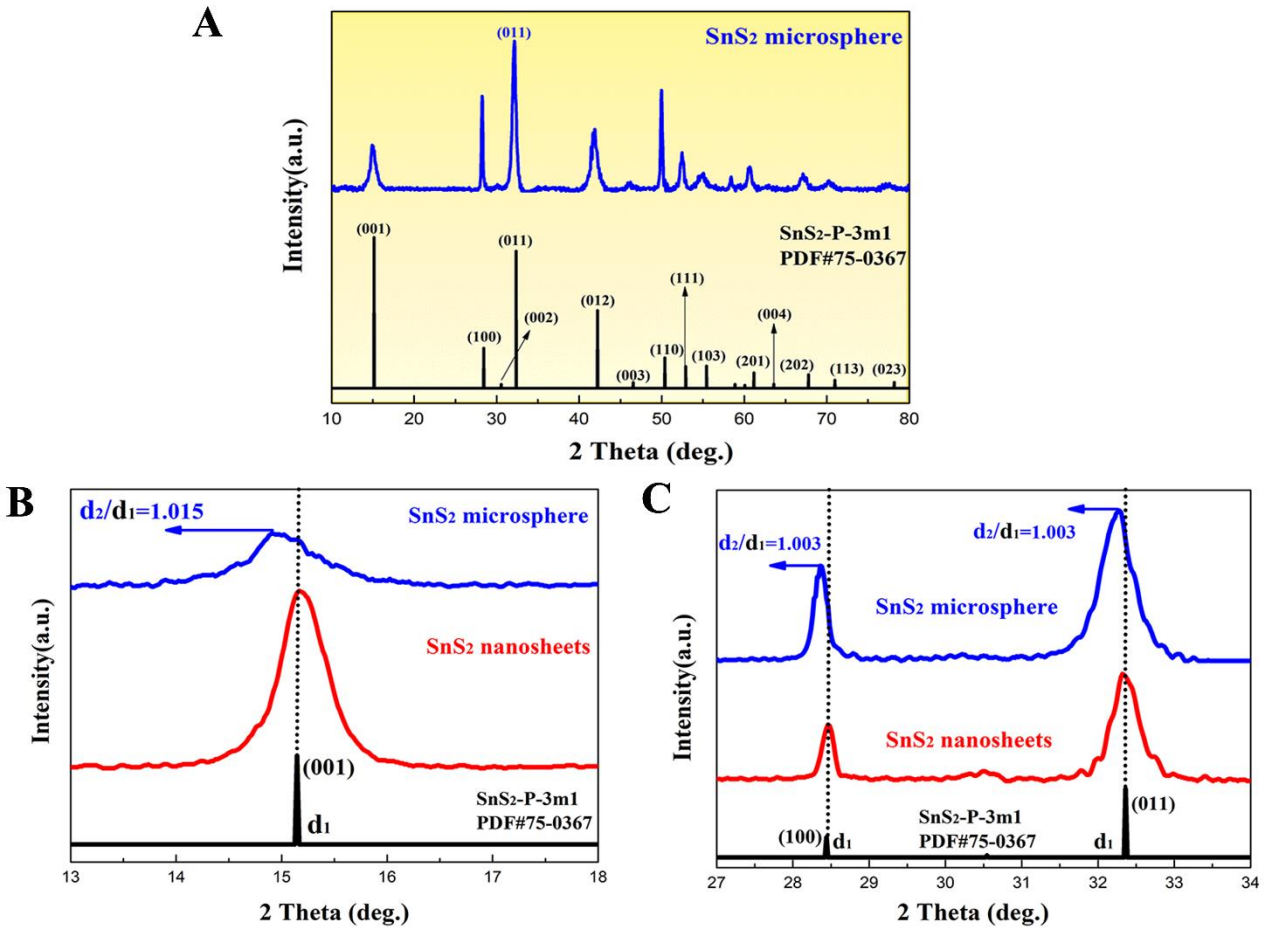

Figure S1. XRD characterization of SnS_2 microspheres.

(A) XRD pattern of SnS_2 microspheres.

(B, C) XRD pattern of SnS_2 microspheres and SnS_2 nanosheets with 2θ angle of 13°-18° and 27°-34°.

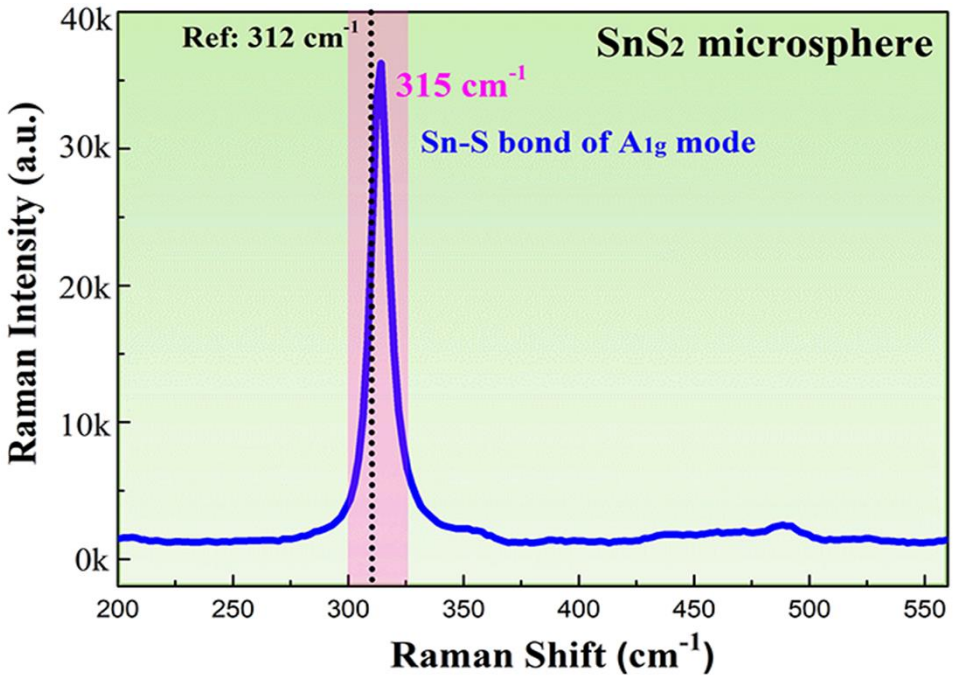

Figure S2. Raman spectra of SnS_2 microspheres.

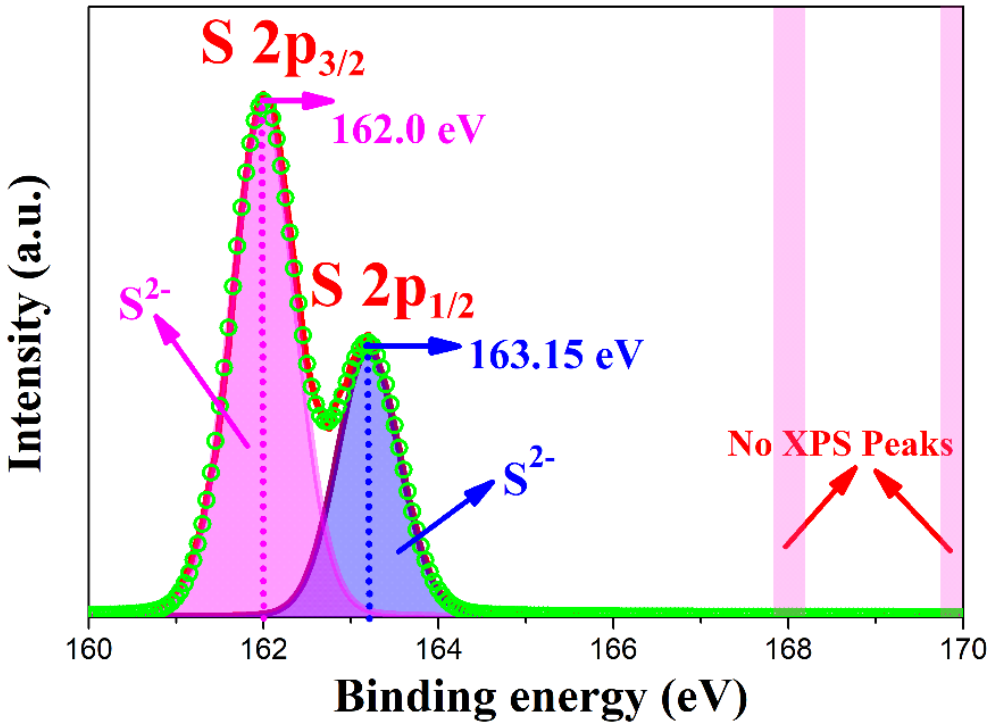

Figure S3. S2*p* XPS spectrum ranging from 160 eV to 170 eV of SnS_2 microspheres.

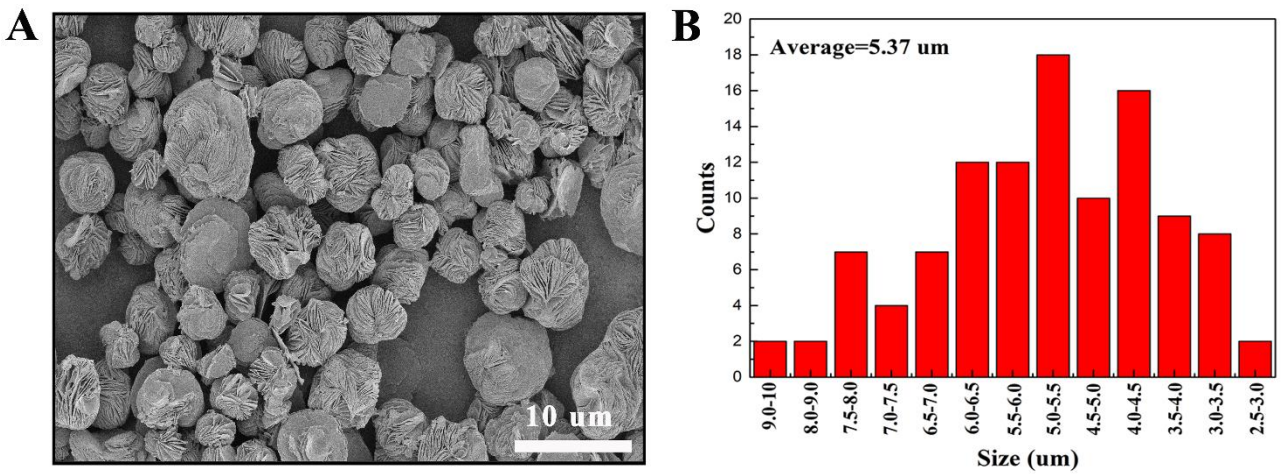

Figure S4. Morphology characterization of SnS_2 microspheres.

(A) The low-magnification SEM image of SnS_2 microspheres.

(B) The statistical size of SnS_2 microspheres.

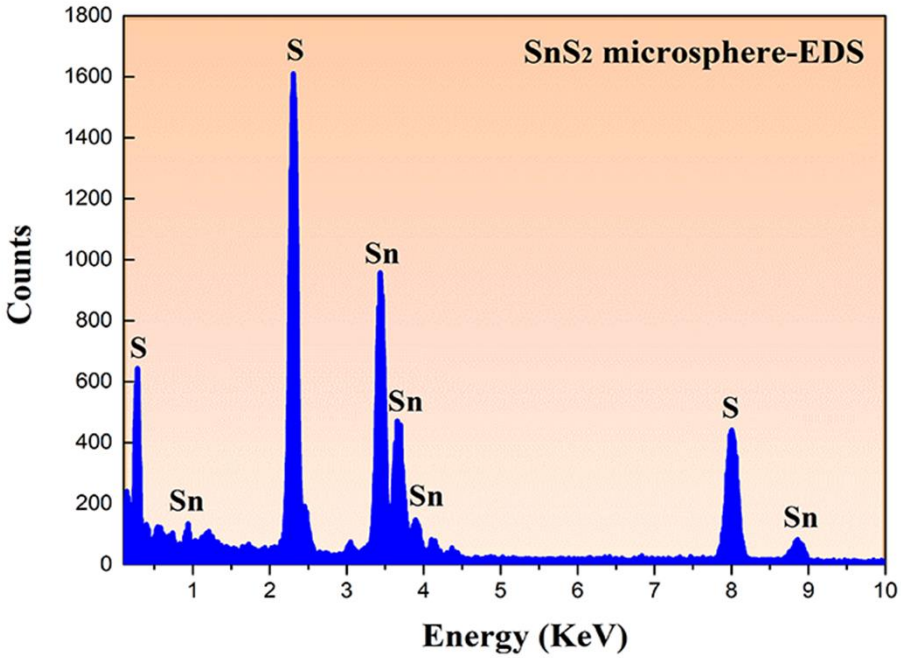

Figure S5. EDS spectrum of SnS_2 microspheres.

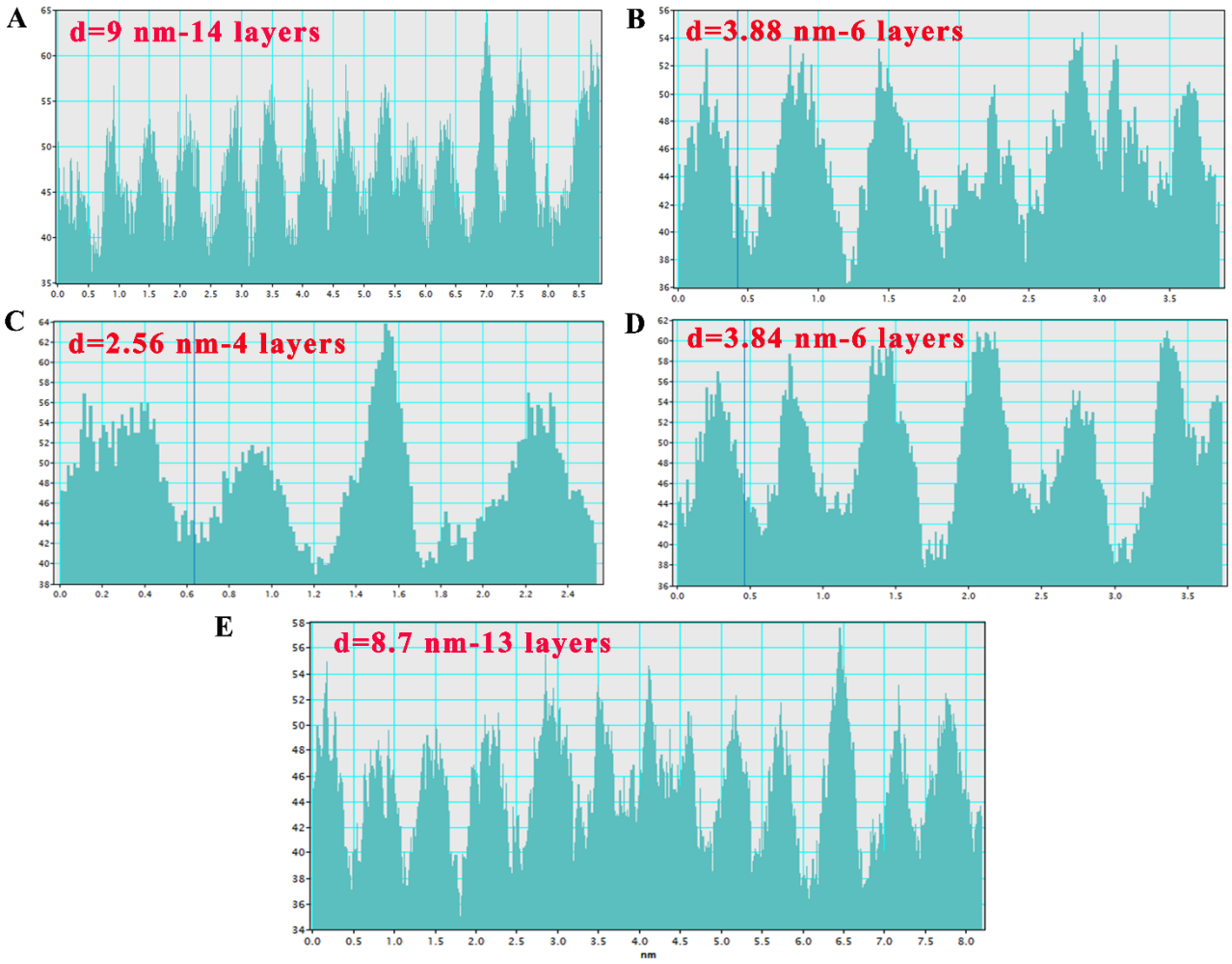

Figure S6. The evidence of lattice fringe space.

(A-E) The lattice fringe space of HRTEM images in Figure 2G for SnS_2 microspheres.

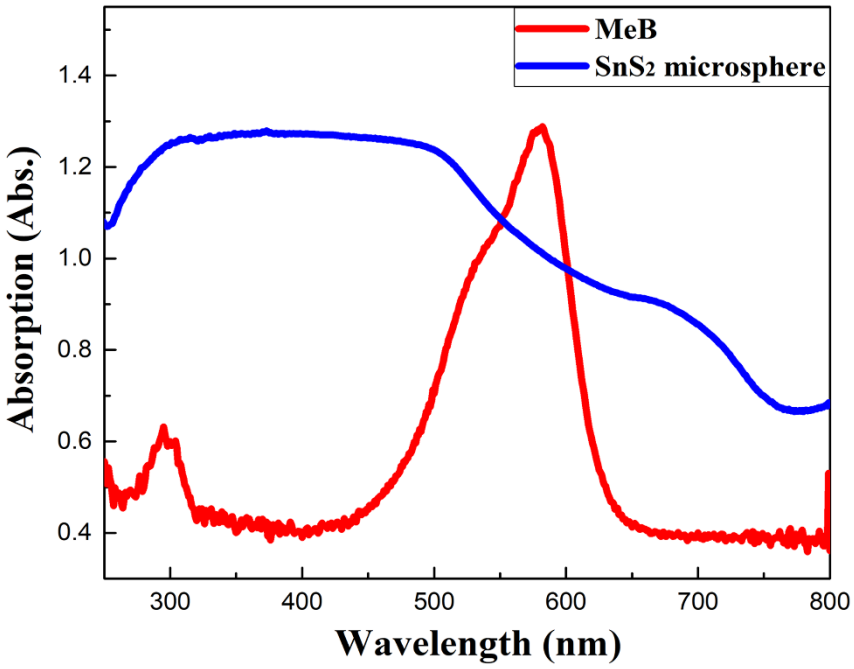

Figure S7. UV-vis optical absorption spectrum of SnS_2 microspheres and MeB molecules.

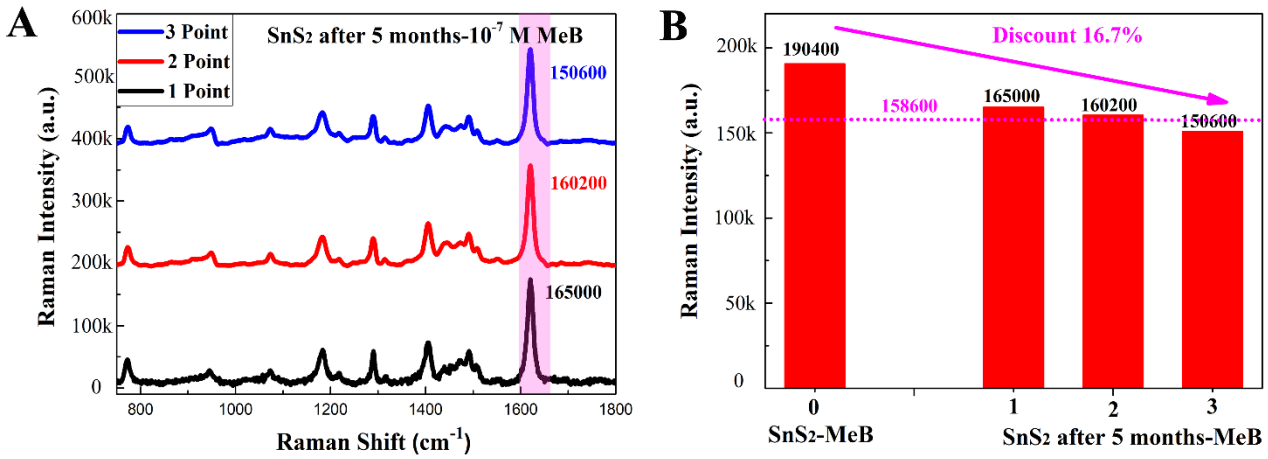

Figure S8. The SERS-enhanced stability of SnS_2 microsphere.

(A) Raman spectra of 10^{-7} M MeB on SnS_2 microsphere after 5 months.

(B) Comparison of Raman intensity for MeB molecules on fresh SnS_2 microsphere and SnS_2 microsphere after 5 months

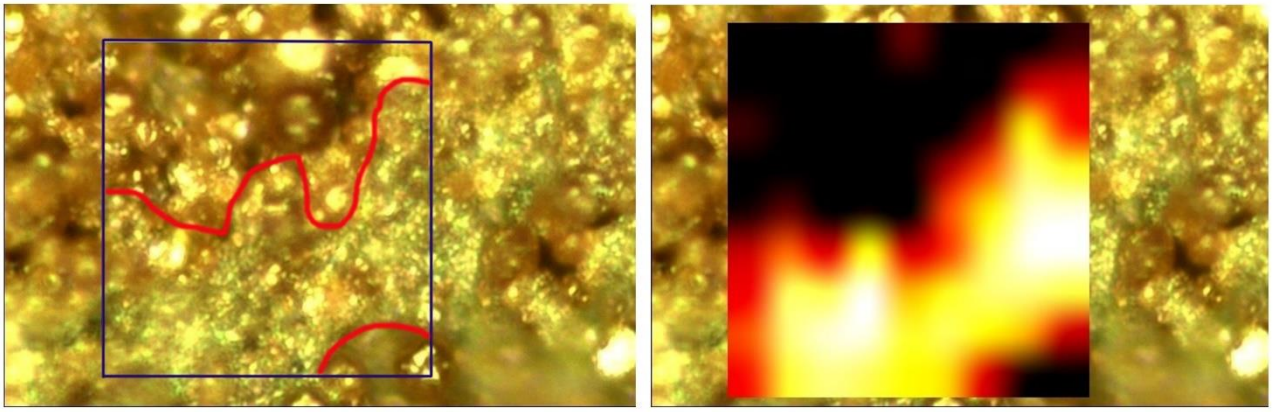

Figure S9. Raman mapping images with 72×48 μm^2 region of 10^{-10} M MeB on SnS_2 microspheres.

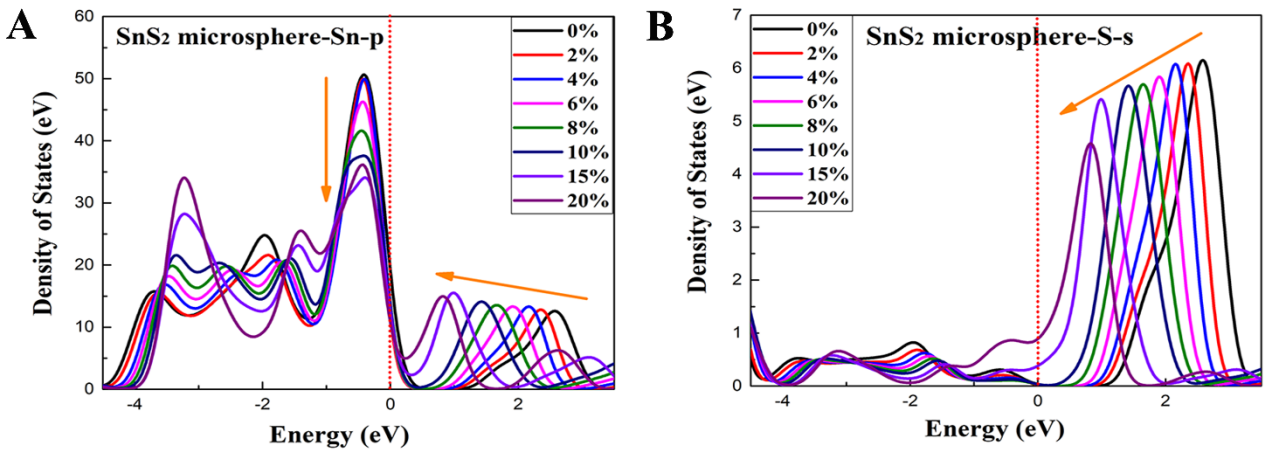

Figure S10. The electronic structure of SnS_2 crystal with tensile strain based on DFT calculations.

(A) Density of states of Sn-p orbitals in the hexagonal SnS_2 crystal with 0%-20% tensile strain.

(B) Density of states of S-s orbitals in the hexagonal SnS_2 crystal with 0%-20% tensile strain.

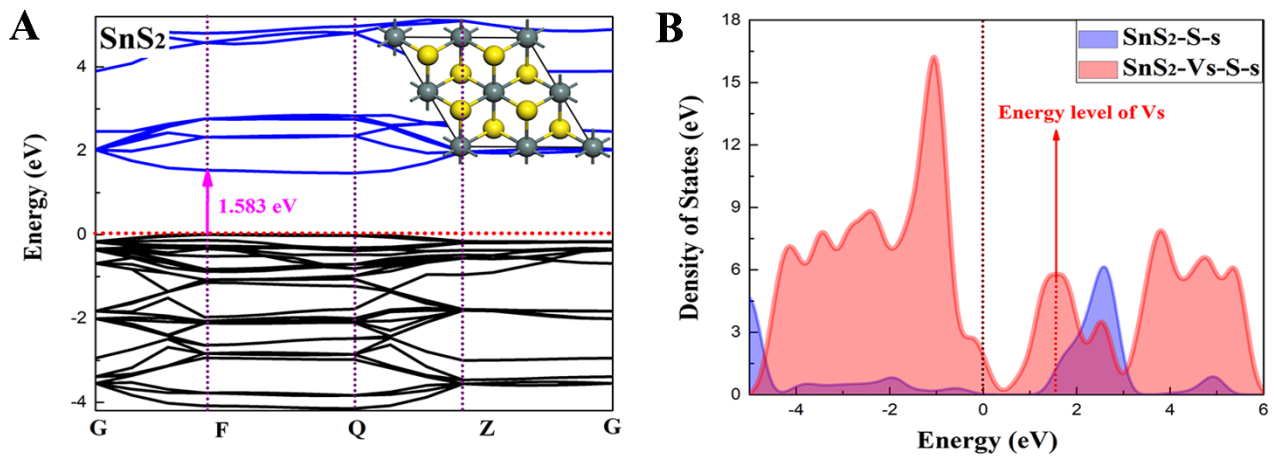

Figure S11. The electronic structure of SnS_2 crystal with sulfur vacancies based on DFT calculations.

(A) Band structure of the hexagonal SnS_2 crystal.

(B) Density of states of S s orbitals in the hexagonal SnS_2 crystal with sulfur vacancies.

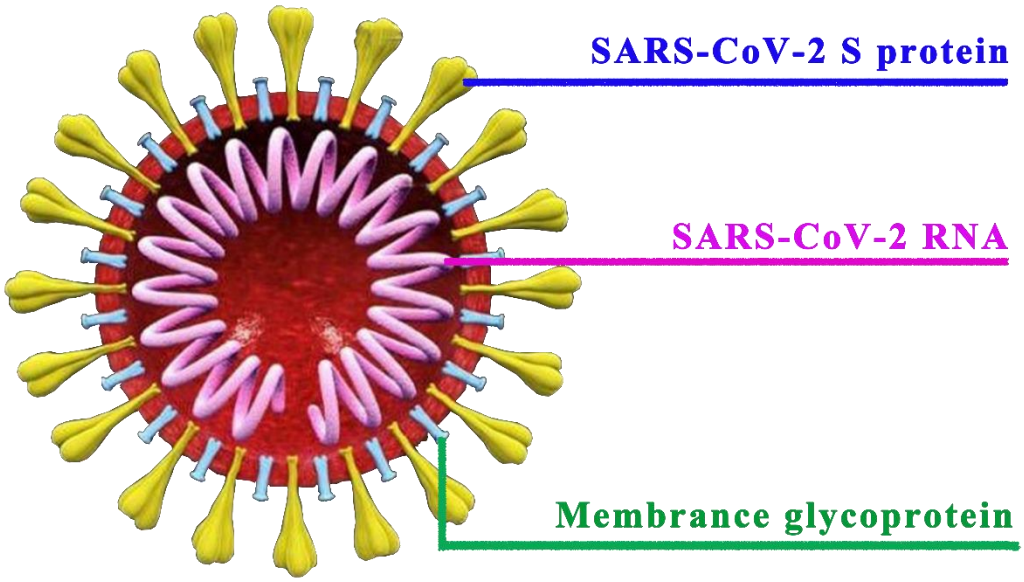

Figure S12. Schematic diagram of composition and structure for SARS-CoV-2.

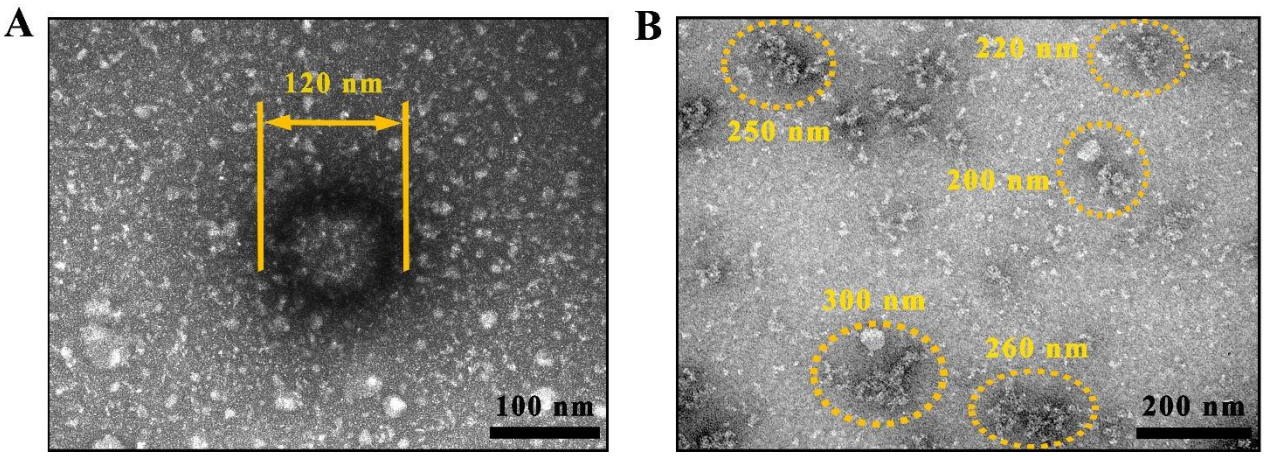

Figure S13. TEM characterization of SARS-CoV-2 viral structure.

(A) TEM images of SARS-CoV-2 with complete viral structure.

(B) TEM images of lysed SARS-CoV-2. The white agglomerates in TEM images are some protein impurities.

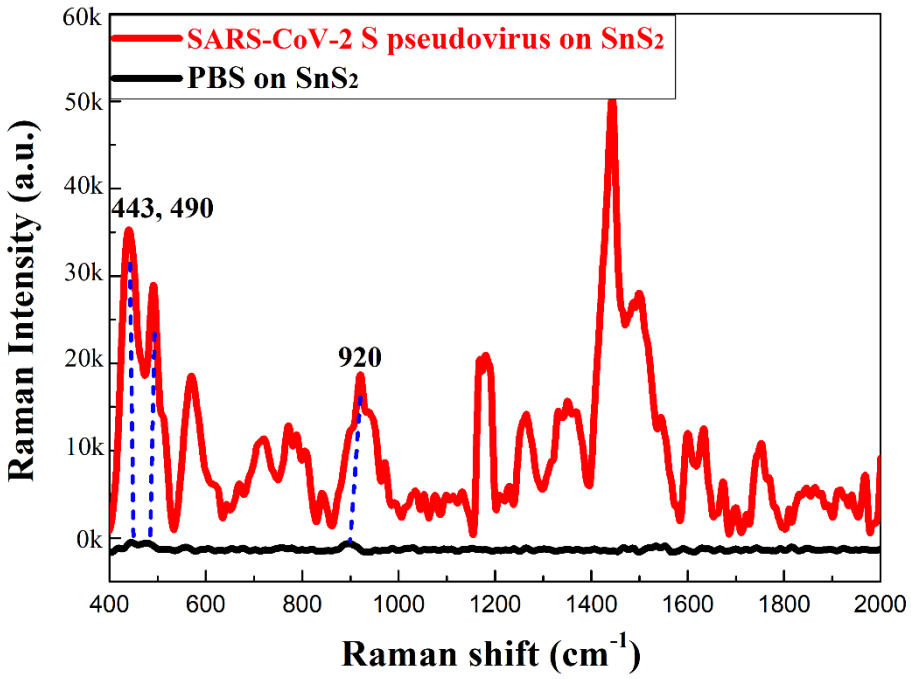

Figure S14. Raman spectra of SARS-CoV-2 S pseudovirus and PBS on SnS_2 microspheres.

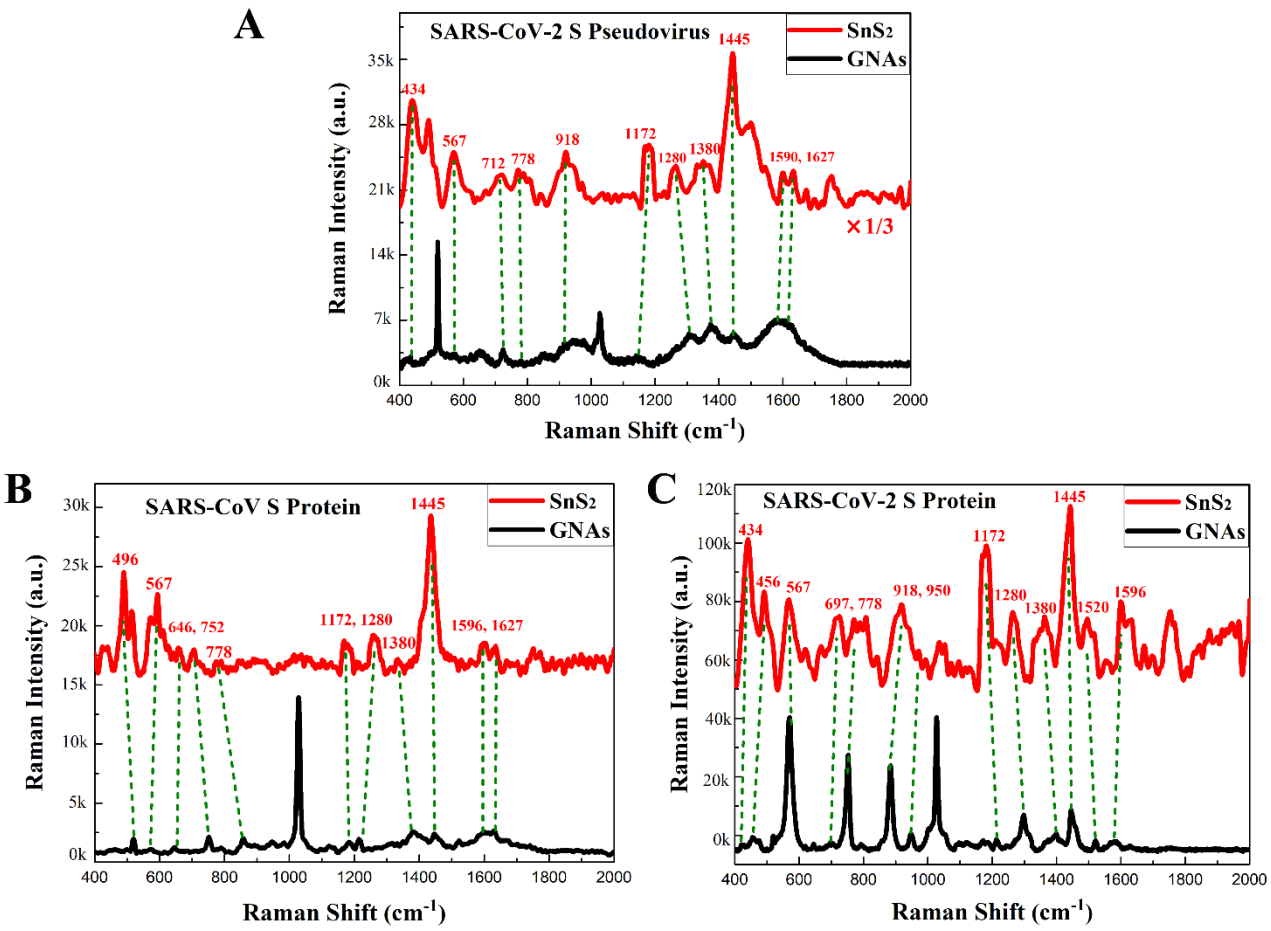

Figure S15. The accuracy research of viral Raman spectra.

(A) Raman spectra of SARS-CoV-2 S pseudovirus on SnS_2 microspheres and Au substrates.

(B) Raman spectra of SARS-CoV S protein on SnS_2 microspheres and Au substrates.

(C) Raman spectra of SARS-CoV-2 S protein on SnS_2 microspheres and Au substrates.

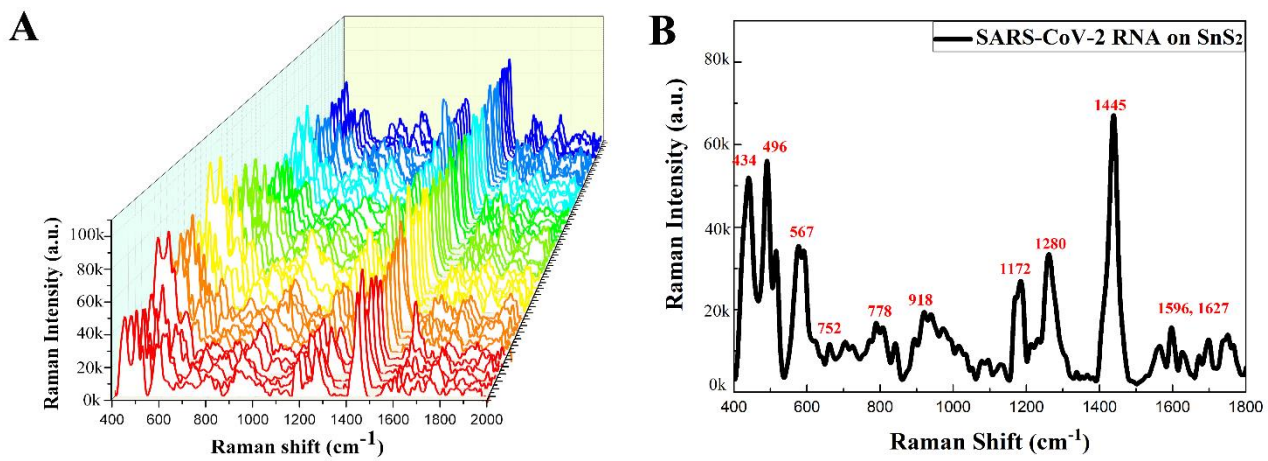

Figure S16. Raman spectra of SARS-CoV-2 RNA.

(A) Raman spectra of 46 measured points for SARS-CoV-2 RNA on SnS_2 microspheres.

(B) Raman spectra of SARS-CoV-2 RNA.

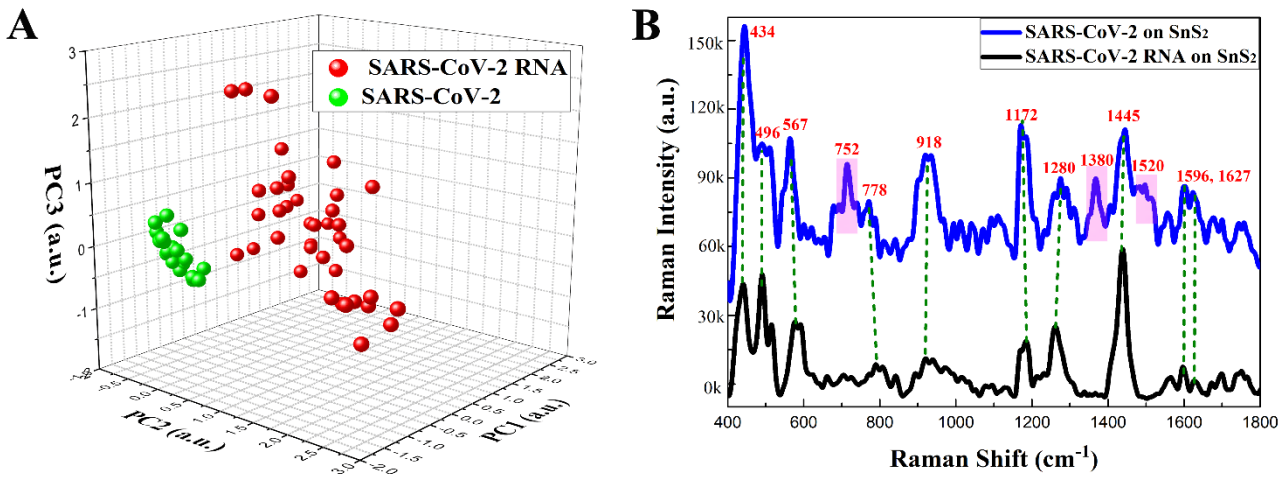

Figure S17. PCA and Raman peaks analysis of SARS-CoV-2 RNA and SARS-CoV-2.

(A) The key features of SERS patterns to classify the SARS-CoV-2 RNA and SARS-CoV-2.

(B) Raman spectra of SARS-CoV-2 RNA and SARS-CoV-2.

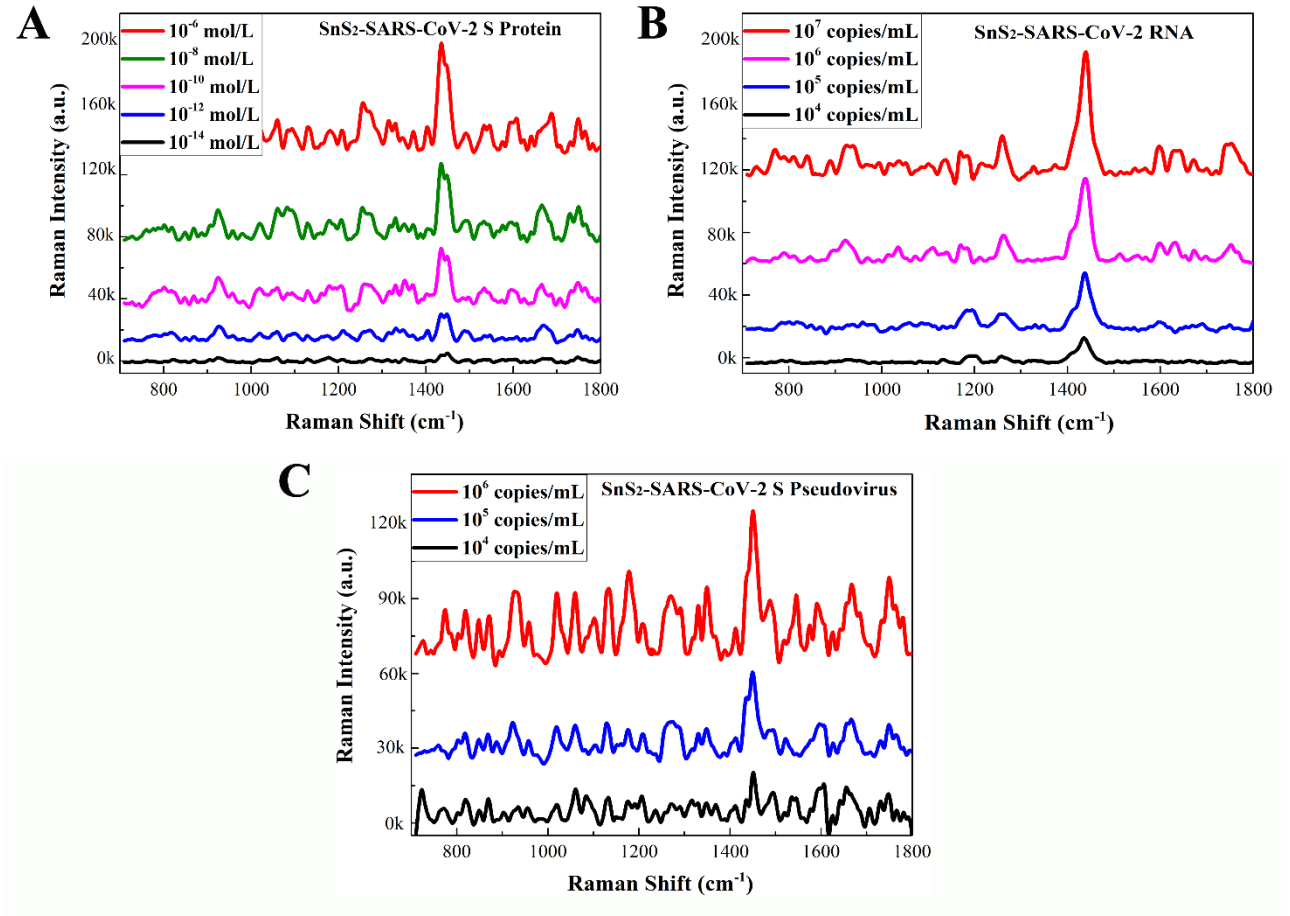

Figure S18. The limits of detection for three physical forms of SARS-CoV-2 virus.

(A) Raman spectra of 10^{-6}-10^{-14} mol/L SARS-CoV-2 S protein on SnS_2 microspheres.

(B) Raman spectra of 10^{4}-10^{7} copies/mL SARS-CoV-2 RNA on SnS_2 microspheres.

(C) Raman spectra of 10^{4}-10^{6} copies/mL SARS-CoV-2 S pseudovirus on SnS_2 microspheres.

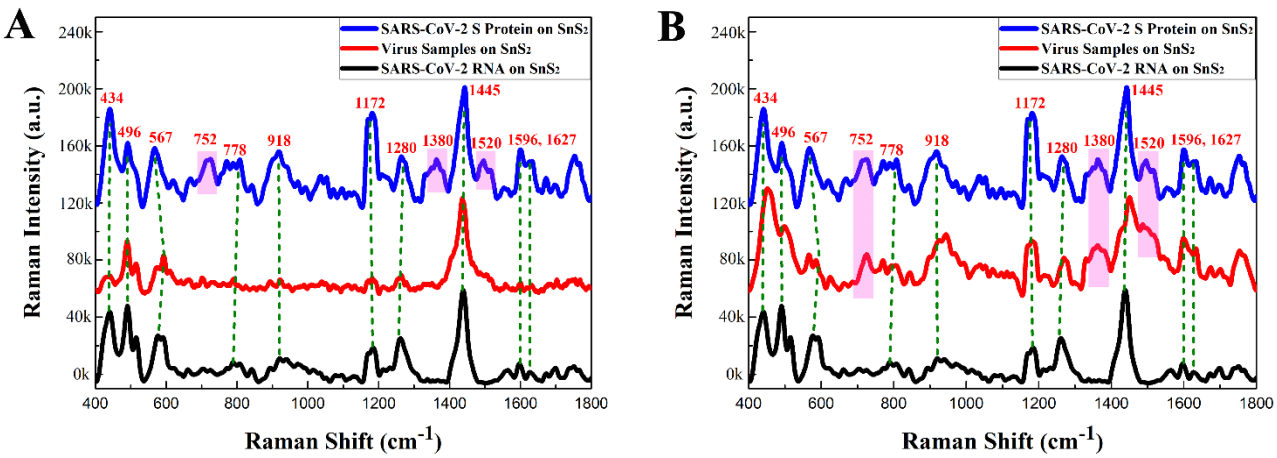

Figure S19. Comparison of Raman peaks for SARS-CoV-2 virus samples.

(A) Raman spectra of virus samples being identified to SARS-CoV-2 RNA.

(B) Raman spectra of virus samples SARS-CoV-2 being identified to SARS-CoV-2 S protein.

A

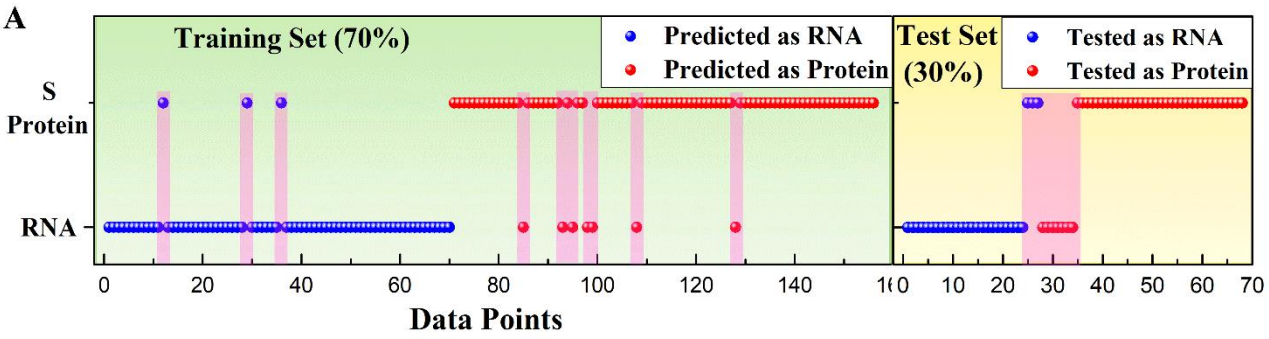

B

Classification		Training Set (70%)		Total	Test Set (30%)		Total
		Original Class			Original Class		
		RNA	S Protein		RNA	S Protein	
Predicted Class	RNA	67	7		24	7	
	S Protein	3	79		3	44	
	Accuracy	95.71%	91.86%	93.59%	88.89%	86.27%	85.29%

C

Classification Results			
Classification	Predicted Group		Total
	RNA	S Protein	
RNA	48	0	48
S Protein	0	31	31
Samples	57	98	156

Figure S20. The SVM analyzed results of virus sample with moderate infectious risk.

(A) Confusion matrix of SARS-CoV-2 S protein and RNA for the mixture of the complete-structure and the lysed SARS-CoV-2 after RNA elimination and re-lysis.

(B) Predicted labels of test set for SARS-CoV-2 S protein and RNA for the complete-structure and the lysed SARS-CoV-2 after RNA elimination and re-lysis.

(C) Classification results of viral samples for SARS-CoV-2 S protein and RNA based on Support Vector Machine (SVM) method.

A

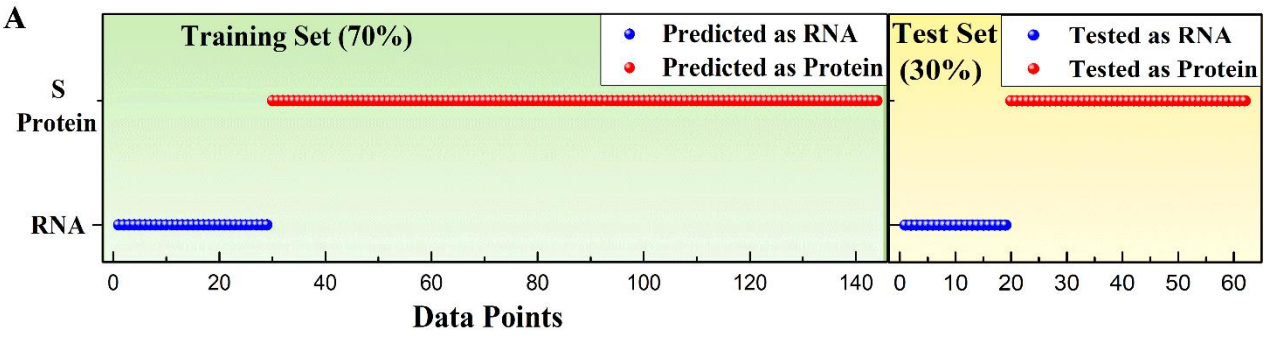

B

Classification		Training Set (70%)		Total	Test Set (30%)		Total
		Original Class			Original Class		
		RNA	S Protein		RNA	S Protein	
Predicted Class	RNA	29	0		19	0	
	S Protein	0	115		0	43	
	Accuracy	100.0%	100.0%	100.0%	100.0%	100.0%	100.0%

C

Classification Results			
Classification	Predicted Group		Total
	RNA	S Protein	
RNA	48	0	48
S Protein	0	31	31
Samples	0	127	127

Figure S21. The SVM analyzed results of virus sample with non-infectious risk.

(A) Confusion matrix of SARS-CoV-2 S protein and RNA for the lysed SARS-CoV-2 after RNA elimination and re-lysis.

(B) Predicted labels of test set for SARS-CoV-2 S protein and RNA for the lysed SARS-CoV-2 after RNA elimination and re-lysis.

(C) Classification results of viral samples for SARS-CoV-2 S protein and RNA based on Support Vector Machine (SVM) method.

SI-1. Raman vibration modes and SERS EFs of MeB

Table S1. Raman shifts of SERS characteristic peaks and corresponding assignments and EFs.

Raman shift (cm^{-1}) of MeB	**EF**	**Assignments**
1620	3.0×10^8	ν_{as} $(CCC)_{ring}$
1405	5.0×10^7	ν_s(C-N)
1182	6.0×10^7	ρ_τ(C-H)
1072	1.3×10^{10}	ρ_{ipb} $(CC_{center}C)$
772	5.5×10^7	$\nu_{as}(CN_{center}C)$

ν, stretching; ρ_τ, twisting vibrations; ρ_{ipb}, in-plane deformation; (s, symmetric; as, asymmetric)

SI-2. The calculation of enrichment multiples

In order to explore the physical enrichment of SnS_2 microspheres, we immersed SnS_2 powder in the MeB solution and dropped MeB solution on SnS_2 substrates for Raman detection. In detail, the 0.01 g of the synthesized SnS_2 microspheres was immersed in 30 mL of 10^{-7} M MeB aqueous solution and a dose of mixture solution with a volume of 5 μL after centrifugation was dropped on the surface of glass substrate, dried at room temperature for Raman detection. On another way, a volume of 5 μL for 10^{-7} M MeB solution was dropped on the synthesized SnS_2 microspheres substrates and dried at room temperature for Raman detection. Then, their Raman spectra were detected and the average number N_{SERS} of MeB molecules on SnS_2 microspheres in the Raman detection region was calculated to explore the physical enrichment of SnS_2 microspheres.

As for immersing SnS_2 powder in the 10^{-7} M MeB, $EF_1 = \frac{I_{SERS-1}}{I_{prob}} \times \frac{N_{prob}}{N_{SERS-1}}$;

As for dropping MeB on SnS_2 substrates, $EF_2 = \frac{I_{SERS-2}}{I_{prob}} \times \frac{N_{prob}}{N_{SERS-2}}$.

Theoretically, if we ignore the molecular enrichment effect, SnS_2 microspheres should show the same SERS enhancement factor for MeB molecule with the same concentration, that is $EF_1 = EF_2$.

$$\frac{I_{SERS-1}}{I_{prob}} \times \frac{N_{prob}}{N_{SERS-1}} = \frac{I_{SERS-2}}{I_{prob}} \times \frac{N_{prob}}{N_{SERS-2}}$$

$$\frac{N_{SERS-1}}{N_{SERS-2}} = \frac{I_{SERS-1}}{I_{SERS-2}} = \frac{4957650.07}{125098.17} \approx 40$$

Therefore, the physical enrichment of SnS_2 microspheres is $N_{SERS-1}/N_{SERS-2} = 40$.

SI-3. Enhancement factor (EF) calculations

SERS enhancement factors of SnS_2 microspheres substrates for MeB were calculated by the following general formula:

$$EF=\frac{I_{SERS}}{I_{prob}}\times\frac{N_{prob}}{N_{SERS}} \quad (1)$$

Based on formula (1), I_{SERS} and I_{prob} are the Raman intensity at a selected Raman peak of molecule-semiconductor complex and MeB probe molecules. N_{SERS} is the average number of MeB molecules on SnS_2 microspheres in the Raman detection region. N_{prob} is the average number of MeB powder in the Raman detection region. In the Raman scattering detection region.

As for the average number N_{SERS-1} of MeB molecules with SERS enhancement:

$$N_{SERS-1}=\frac{C_{sol}V_{sol}N_AA_{Raman}}{A_{substrate}} \quad (2)$$

As for the average number N_{SERS-2} of MeB molecules with SERS enhancement under the effect of molecular enrichment:

$$N_{SERS-2}=40\times N_{SERS-1}=\frac{40\times C_{sol}V_{sol}N_AA_{Raman}}{A_{substrate}} \quad (3)$$

As for the average number of MeB powder without SERS enhancemnt:

$$N_{prob}=C_{prob}hN_AA_{Raman} \quad (4)$$

Where C_{sol} (mol/L) is the concentration of the measured molecular solution, which is 10^{-13} M. And V_{sol} (L) is the volume of the solution that finally dropped on the glass slide after immersing MeB on SnS_2 microspheres powder, which is about 5 μL. A_{Raman} and $A_{substrate}$ (m^2) are the area of laser radiation and droplet diffusion of MeB and SnS_2 microspheres powder complex on the glass slide, respectively. And the circle diameter of droplet diffusion for MeB and SnS_2 microspheres powder complex is 0.8 cm. C_{prob} of MeB powder is 3.13 M. h is the laser radiation depth, which is 21 μm.[1]

$$\frac{N_{prob}}{N_{SERS-2}}=\frac{C_{prob}hN_AA_{Raman}A_{substrate}}{40\times C_{sol}V_{sol}N_AA_{Raman}}=\frac{C_{prob}hA_{substrate}}{C_{sol}V_{sol}}$$

$$=\frac{3.13\times 2.1\times 10^{-5}\times\pi\times 0.16\times 10^{-4}}{40\times 5\times 10^{-6}\times 10^{-13}}=1.66\times 10^{8}$$

Under the excitation of 785 nm laser, the Raman intensity I_{prob} of MeB powder at 1620 cm^{-1} is 201710.8, and I_{SERS} of MeB molecules with SERS enhancement at 1620 cm^{-1} is 363575.4. All Raman spectra complex were detected with the following test conditions: the irradiation power of excitation light is 300 mW×0.05% of 785 nm, and the light irradiation time of each point is 20 s, as well as the light transmission efficiency of the Raman spectrometer is about 20%. Therefore,

$$EF=\frac{I_{SERS}}{I_{prob}}\times\frac{N_{prob}}{N_{SERS}}=\frac{363575.4}{201710.8}\times 1.66\times 10^{8}=3.0\times 10^{8}$$

Based on above calculations of our works, SERS enhancement factors and the corresponding detection limits of all reported semiconductor-based SERS substrates were summarized in the following table.

Table S2. Reported enhancement factors on different semiconductor nanostructure substrates.

SERS substrates	**Probe molecules**	**Excitation wavelength (nm)**	**EF**	**Detection limits**
Multi-layer Nb_2C MXenes[2]	MeB	532	3.0×10^6	10^{-8} M
Multi-layer Ta_2C MXenes[2]	MV	532	1.4×10^6	10^{-7} M
Multi-layer Ti_3C_2 MXenes[3]	MeB	785	3.2×10^6	10^{-7} M
Monolayer of Ti_3C_2 MXene[4]	R6G	532	3.82×10^8	10^{-11} M
ZnSe nanoparticles[5]	4-Mpy	514.5	2×10^6	10^{-3} M
Amorphous TiO_2 nanosheets[6]	4-MBA	633	1.86×10^6	6×10^{-6} M
sea urchin-like $W_{18}O_{49}$[7]	R6G	532.8	3.4×10^5	10^{-7} M
Porous ZnO nanosheets[8]	4-MBA	514.5	10^3	10^{-6} M
Amorphous MoO_3[9]	R6G	532	1.8×10^7	10^{-8} M
Nanosphere Cu_2O[10]	R6G	514.5	8×10^5	6×10^{-9} M
Mo-doping Ta_2O_5 nanowires[1]	MV	532	2.2×10^7	9×10^{-9} M
Nb_2O_5 nanoflowers[11]	MV	532	7.1×10^7	10^{-8} M
Amorphous Rh_3S_6 microbowls[12]	R6G	647	10^5	10^{-7} M
Metal-Like $H_{1.68}MoO_3$[13]	R6G	633	1.1×10^7	10^{-9} M
Mo_2N flexible membrane[14]	2,4-DCP	532	5.2×10^7	10^{-11} M
MoN nanosheets[15]	R6G	633	8.2×10^6	10^{-10} M
$NbTe_2$ nanosheets[16]	MB	514	5.6×10^6	10^{-9} M
MoS_2@ZnO heterojunction[17]	MB	514	1.2×10^6	10^{-12} M
SnS_2 microspheres (in this work)	MeB	785	3.0×10^8	10^{-13} M

SI-4. Gene sequence of S protein for SARS-CoV-2 and SARS-CoV

The S protein of SARS-CoV-2 is similar to that of SARS-CoV, showing only 74.6% identity in their amino acid sequences. Their SERS spectra exhibit significant different characteristics peaks.

Gene sequence of SARS-CoV-2 S protein (Accession: YP_009724390.1)

MFVFLVLLPLVSSQCVNLTTRTQLPPAYTNSFTRGVYYPDKVFRSSVLHSTQDLFLPFFSNVTWFHAIHVSGTN
GTKRFDNPVLPFNDGVYFASTEKSNIIRGWIFGTTLDSKTQSLLIVNNATNVVIKVCEFQFCNDPFLGVYYHKN
NKSWMESEFRVYSSANNCTFEYVSQPFLMDLEGKQGNFKNLREFVFKNIDGYFKIYSKHTPINLVRDLPQGFS
ALEPLVDLPIGINITRFQTLLALHRSYLTPGDSSSGWTAGAAAYYVGVLQPRTFLLKYNENGTITDAVDCALDP
LSETKCTLKSFTVEKGIYQTSNFRVQPTESIVRFPNITNLCPFGEVFNATRFASVYAWNRKRISNCVADYSVLYN
SASFSTFKCYGVSPTKLNDLCFTNVYADSFVIRGDEVRQIAPGQTGKIADYNYKLPDDFTGCVIAWNSNNLDS
KVGGNYNYLYRLFRKSNLKPFERDISTEIYQAGSTPCNGVEGFNCYFPLQSYGFQPTNGVGYQPYRVVVLSFE
LLHAPATVCGPKKSTNLVKGCVIAWNSNNLDSKVGGNYNYLYRLFRKSNLKPFERDISTEIYQAGSTPCNGVE
GFNCYFPLQSYGFQPTNGVGYQPYRVVVLSFELLHAPATVCGPKKSTNLVKNKCVNFNFNGLTGTGVLTESN
KKFLPFQQFGRDIADTTDAVRDPQTLEILDITPCSFGGVSVITPGTNTSNQVAVLYQDVNCTEVPVAIHADQLTP
TWRVYSTGSNVFQTRAGCLIGAEHVNNSYECDIPIGAGICASYQTQTNSPRRARSVASQSIIAYTMSLGAENSV
AYSNNSIAIPTNFTISVTTEILPVSMTKTSVDCTMYICGDSTECSNLLLGYGSFCTQLNRALTGIAVEQDKNTQE
VFAQVKQIYKTPPIKDFGGFNFSQILPDPSKPSKRSFIEDLLFNKVTLADAGFIKQYGDCLGDIAARDLICAQKFN
GLTVLPPLLTDEMIAQYTSALLAGTITSGWTFGAGAALQIPFAMQMAYRFNGIGVTQNVLYENQKLIANQFNS
AIGKIQDSLSSTASALGKLQDVVNQNAQALNTLVKQLSSNFGAISSVLNDILSRLDKVEAEVQIDRLITGRLQSL
QTYVTQQLIRAAEIRASANLAATKMSECVLGQSKRVDFCGKGYHLMSFPQSAPHGVVFLHVTYVPAQEKNFT
TAPAICHDGKAHFPREGVFVSNGTHWFVTQRNFYEPQIITTDNTFVSGNCDVVIG
IVNNTVYDPLQPELDSFKEELDKYFKNHTSPDVDLGDISGINASVVNIQKEIDRLNEVAKNLNESLIDLQELGKY
EQYIKWPWYIWLGFIAGLIAIVMVTIMLCCMTSCCSCLKGCCSCGSCCKFDEDDSEPVLKGVKLHYT

Gene sequence of SARS-CoV S protein (Accession: YP_009825051.1)

MFIFLLFLTLTSGSDLDRCTTFDDVQBNVTQHTSSMRGVYYPDEIFRSDTLYLTQDLFLPFYSNVTGFHTINHTF
GNPVIPFKDGIYFAATEKSNVVRGWVFGSTMNNKSQSVIIINNSTNVVIRACNFELCDNPFFAVSKPMGTQTHT
MIFDNAFNCTFEYISDAFSLDVSEKSGNFKHLREFVFKNKDGFLVVVKGYQPIDVVRDLPSGFNTLKPIFKLPLG
INITNFRAILTAFSPAQDIWGTSAAAVFVGYLKPTTFMLKYDENGTITDAVDCSQNPLAELKCSVKSFEIDKGIY
QTSNFRVVPSGDVVRFPNITNLCPFGEVFNATKFPSVVAWERKKISNCVADYSVLYNSTFFSTFKCYGVSATKL
NDLCFSNVYADSFVVKGDDVRQIAPGQTGVIADYNYKLPDDFMGCVLAWNTRNIDATSTGNYNYKYRYLRH
GKLRPFERDISNVPFSPDGKPCTPALNCYWPLNDYGFYTTTGIGYQPYRVVVLSFELLNAPATVCGPKLSTDLI
KNQCVNFNFNGLTGTGVLTPSSKRFQPFQQFGRDVSDFTDSVRDPKTSEILDISPCAFGGVSVITPGTNASSEVA
VLYQDVNCTDVSTAIHADQLTPAWRIYSTGNNVFQTQAGCLIGAEHVDTSYECDIPIGAGICASYHTVSLLRST
SQKSIVAYTMSLGADSSIAYSNNTIAIPTNFSISITTEVMPVSMAKTSVDCNMYICGDSTECANLLLQYGSFCTQ
LNRALSGIAAEQDRNTREVFAQVKQMYKTPTLKYFGGFNFSQILPDPLKPTKRSFIEDLLFNKVTLADAGFMK
QVGECLGDINARDLICAQKFNGLTVLPPLLTDDMIAAYTAALVSGTATAGWTFGAGAALQIPFAMQMAYRFN
GIGVTQNVLYENQKQIANQFNKAISQIQESLTTTSTALGKLQDVVNQNAQALNTLVKQLSSNFGAISSVLNDIL
SRLDKVEAEVQIDRLITQRLQSLQTYVTQQLIRAAEIRASANLAATKMSECVLGQSKRVDFCGKGYHLMSFPQ
AAPHGVVFLHVTYVPSQERNFTTAPAICHEGKAYFPREGVFNGTSWFITQRNFFSPQIITTDNTFVSGNCDVVIG

IINNTVYDPLQPELDSFKEELDKYFKNHTSPDVDLGDISGINASVVNIQKEIDRLNEVAKNLNESLIDLQELGKY
EQVIKWPWYVWLGFIAGLIAIVMVTILLCCMTSCCSCLKGACSCGSCCKFDEDDSEPVLKGVKLHYT

Table S3. Raman peak assignments for proteins and virus on GNAs substrates

Assignments (Literature)	**Literature /(cm^{-1})**	**Reference Au /(cm^{-1})**	**Experiment SnS_2 /(cm^{-1})**
Protonated amine group, δ(-NH_3^+)	Ref[20]	454	434
δ(S-S)	518[20]	/	496
Amide V	567[19]	568	567
Trp, v(ϕ)	758[18]	752	752
Cys, v(C-C-N)	840[23]	/	778
Skeleton, v(C-C, α-Helix)	Ref[20]	950	918
Trp & Phe, v(C-C_6H_5)	1209[18]	1214	1172
Amide III, v (C-N), δ (N-H)	1300[21]	1296	1280
Trp, W7 [v(N_1–C_8)]	1365[19]	1380	1380
Nucleic Acids (DNA or RNA), proteins and lipids, v (C-H), b (N-H)	1450-1470[18,20]	1445	1445
Amide II, ρ_{ipb} (N-H, C-O)	1515[21] 1509-1552, 1529[22]	1521	1520
Tyr & Phe, v(ϕ)	1591[20]	1592	1596
v(C=C)	1617-1680[18]	1626	1627

Abbreviation: δ, deformation; v, stretching; ρ_{τ}, twisting vibrations; ϕ, aromatic ring; ρ_{ipb}, in-plane deformation; B bending vibration

SI-5. The definition of three existed forms for SARS-CoV-2 in this work

In this work, we defined three forms of SARS-CoV-2 virus and descripted their characteristics of viral structure.

(1) The active or un-lysed SARS-CoV-2 means that the virus has not been heated treatment, which exhibits a complete viral structure and high viral infectivity (as shown in the Schematic diagram A below). And its Raman spectra shows the characteristic Raman peaks of SARS-CoV-2 S protein.

(2) The SARS-CoV-2 with complete viral structure means that the virus has been heated at 45 ℃ for 10 min. Its spatial configuration and surface protein structure are still maintaining, only the viral activity and infectivity are reduced (as shown in the Schematic diagram B below). It is an incompletely inactivated virus, and its Raman spectra shows the characteristic Raman peaks of SARS-CoV-2 S protein.

(3) The lysed SARS-CoV-2 means that the virus was treated by the lysing process of ultrasound, whose virus structure and spatial configuration are destroyed, and the nucleic acids (RNA) and other proteins originally wrapped in the envelope are exposed or released outside the virus particle (as shown in the Schematic diagram C below). This lysed SARS-CoV-2 sample is non-infectious, and presents both the characteristic Raman peaks of SARS-CoV-2 S protein and RNA.

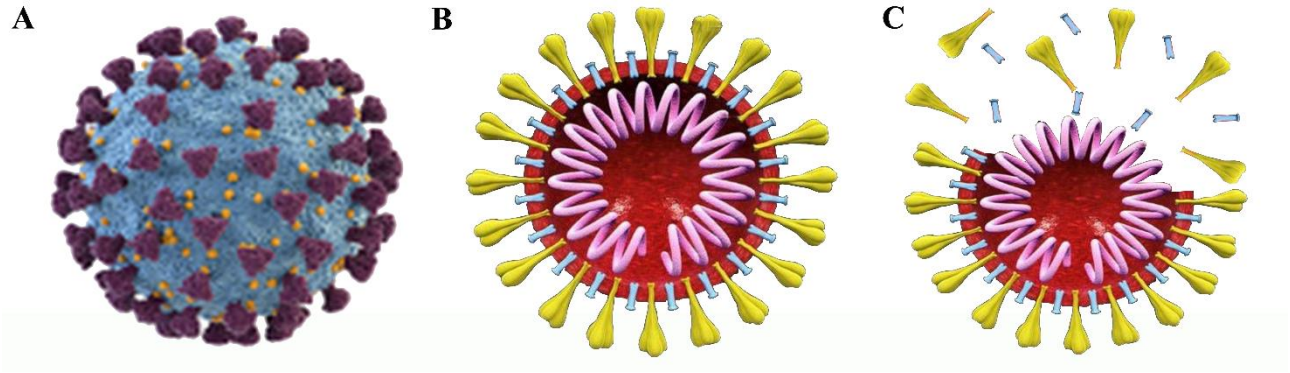

Schematic diagram of composition and structure for the active or un-lysed SARS-CoV-2 (A), the SARS-CoV-2 with complete viral structure (B), the lysed SARS-CoV-2 (C).

II-Supplemental Experimental Procedures

Preparation of SnS_2 microspheres

SnS_2 microspheres were synthesized through a simple one-step hydrothermal reaction with no surfactant or template agent adding. The microspheres morphology are directly formed by curling nanosheets through adjusting the concentration of reactants. Firstly, 1.6 g of thioacetamide (TTA) was dissolved in 55 mL of deionized water under electromagnetic stirring at 60 °C for about 10 minutes, and obtained a mixed transparent solution. The chemical reaction in this dissolution process is $CH_3CSNH_2 + H_2O = CH_3CONH_2 + H_2S$. Then, 0.8 g of $Na_2SnO_3{\cdot}3H_2O$ powder was dissolved in the above TTA solution, and mixed uniformly by electromagnetic stirring to obtain a precursor solution. Finally, above precursor solution was transferred into a 100 mL of PPL-lined stainless-steel autoclave to carry out the hydrothermal reaction at 180 ℃ for 24 hours, and obtain a brown precipitate. The brown precipitate was centrifuged, washed three times with deionized water, and freeze-dried to obtain the brown SnS_2 microspheres powder. The chemical reaction in the hydrothermal reaction is $Na_2SnO_3 + 2H_2S = SnS_2\downarrow + 2NaOH + H_2O$. In the entire hydrothermal reaction, $Na_2SnO_3{\cdot}3H_2O$ provides the Sn source, and thioacetamide provides the S source.

Characterizations

The powder X-ray diffraction (XRD) measurements of SnS_2 microspheres were carried out by using the Rigaku D/MAX-2200 PC XRD system (parameters: Cu Kα radiation, λ = 1.54 Å, 40 mA and 40 kV). The FEI Magellan 400 field emission scanning electron microscopy (FESEM) was used to provide the micro-morphology of SnS_2 microspheres. The transmission electron microscopy (TEM), high-resolution TEM (HRTEM), energy-dispersive X-ray spectroscopy (EDS) and selected area electron diffraction (SAED) images were performed on a JEM-2100F field emission source transmission electron microscope (200 kV). The Thermo Fisher Scientific ESCAlab250 provided the X-ray photoelectron spectroscopy (XPS).

Samples of the SARS-CoV-2 with complete viral structure and the lysed SARS-CoV-2 for TEM analysis were prepared by depositing 5 μl of diluted virions on the processed microvesicle copper net, and then negatively dyed with 1 wt% uranyl acetate solution for 90 sec and dried again. The stained samples were captured by 120 kV scanning transmission electron microscopes (FEI Titan S/TEM) at the Core Facility Center for Life Sciences, University of Science and Technology of China.

SERS measurements

The MeB aqueous solution with the different concentration of 10^{-6}-10^{-13} M were used to investigate the SERS performance of SnS_2 microspheres. For each Raman test, the 0.01 g of synthesized sample powder was immersed in 30 mL of molecule aqueous solution and treated with ultrasound for 2 h. A dose of mixture solution with a volume of 5 μL was dropped on the surface of glass substrate and dried at room temperature. All the Raman spectra of dye molecules were obtained by Renishaw inVia Reflex Raman spectrometer with the laser power of 0.15 mW at 785 nm and the accumulation time was 20 s, and the laser beam was focused to a spot about 1 μm in diameter with a 50× microscope objective. At least three different points on each substrate were tested, and selected the medium intensity of the Raman spectra at 1620 cm^{-1} peak to calculate the SERS EF value and analyze the relationship trend between the Raman intensity and the MeB concentration.

First-principles calculation

The first-principles calculations based on density functional theory (DFT)[24] with the CASTEP program are employed to investigate the electronic structure of SnS_2 hexagonal crystal with lattice strain and sulfur vacancies. Firstly, the supercell expansion of $3 \times 3 \times 1$ for SnS_2 hexagonal crystal structures with lattice strain from 0% to 20% and sulfur

vacancies were built. After geometry optimization, the band structure and density of states were calculated. During the calculation process, we adopted the PBE method in the generalized gradient approximation (GGA) to describe the periodic boundary conditions and the inter-electronic exchange-correlation energy[25]. The interaction potential between ion core and valence electrons was achieved by the ultra-soft potential (Ultrasoft). The cut-off energy of 600 eV in the wave vector K-space and the Brillouin zone of $4 \times 4 \times 5$ was chosen according to the special K-point of Monkhorst-Park[26]. The calculation accuracy of the crystal structure system reaching the convergence state is set as follows: the total energy change of the system stable within 10^{-6} eV, the force acting on each atom in the unit cell less than 0.005 eV/Å, the residual stress of the unit cell and the tolerance deviation within 0.02 GPa and 10^{-3} Å, respectively.

Machine-learning method based on PCA and Support Vector Machine (SVM)

The Python and Statistical Product & Service Solutions were used to perform Principal Component Analysis (PCA) between SARS-CoV-2 S protein and SARS-CoV S protein, SARS-CoV-2 RNA and SARS-CoV-2. According to PCA, we can get the main difference of Raman spectra for various physical forms of SARS-CoV-2 and constructed the identification standard between SARS-CoV-2 RNA and SARS-CoV-2 S protein. Then, Support Vector Machine (SVM) was used to classify the unknown-structure SARS-CoV-2 virus samples based on the above identification standard. Here we take 70% and 30% of the training set and test set, respectively. Polynomial kernel function, RBF kernel function and Linear kernel function are chosen to cross-validate the training data and select the linear kernel function with the highest accuracy.

SERS detection for five physical forms of SARS-CoV-2

With respect to the Raman detection for various physical forms of SARS-CoV-2, 5×10^{6} copies/mL of SARS-CoV-2 S pseudovirus, 1.33×10^{-6} mol/L of SARS-CoV-2 S protein, 7.47×10^{-7} mol/L of SARS-CoV S protein, about 10^{7} copies/mL of SARS-CoV-2 RNA and SARS-CoV-2 were detected by absorbing on SnS_2 microspheres substrates. Here, the 2.38 mg/mL of SARS-CoV-2 S protein, 3.73 mg/mL solution of SARS-CoV S protein were purchased from Sanyou Biopharmaceuticals (20 μg/Tube, Shanghai, China) and diluted to 1.5 mL by adding Phosphate-Buffered Saline (PBS) solution. Anhui Provincial Center for Disease Control and Prevention provided the 5×10^{6} copies/mL of SARS-CoV-2 S pseudovirus, 10^{9} copies/mL of SARS-CoV-2 RNA and SARS-CoV-2 and diluted to the concentration of 10^{7} copies/mL by adding non-nuclear water. Then, 0.01 g of SnS_2 powder was immersed in above 50 μL diluted biomolecular solutions of SARS-CoV-2 for 30 min and a dose of mixture solution with a volume of 5 μL after centrifugation process was dropped on the surface of glass substrate for Raman detection.

Preparation procedures of SARS-CoV-2 S pseudovirus and heating treatments of SARS-CoV-2

The production and purification of SARS-CoV-2 spike protein-based pseudovirions is shown below. As shown in the Schematic diagram below, Pseudovirions were produced by co-transfection of 293T cells with SARS-CoV-2 Spike protein expressing vector pcDNA3.1(+)-Opt-S and packaging vector pNL4-3-luc+R-E- through polyetherimide (PEI). The supernatants were harvested at 48 h post-transfection, passed through 0.45 μm filter and centrifuged at 800 × g for 5 min to remove cell debris. In order to get purer pseudovirions, 5×PEG8000 NaCl solution was added to the collected pseudovirions, left at 4℃ overnight, and centrifuged at 4000 g for 20 min next day. The supernatant was finally removed and collected by using 40 μl PBS solution.

According to the reported literature[27], the heating treatment at 45 ℃ for 10 min was adopted to reduce the viral activity and infectivity of SARS-CoV-2. The active SARS-CoV-2 samples came from COVID-19 patients were isolated and cultured in the BSL-3 laboratory and frozen at -80 ℃. It is worthwhile to note that all experiments on SARS-CoV-2 are required to be carried out in the P3 laboratory of Anhui Provincial Center for Disease Control and Prevention.

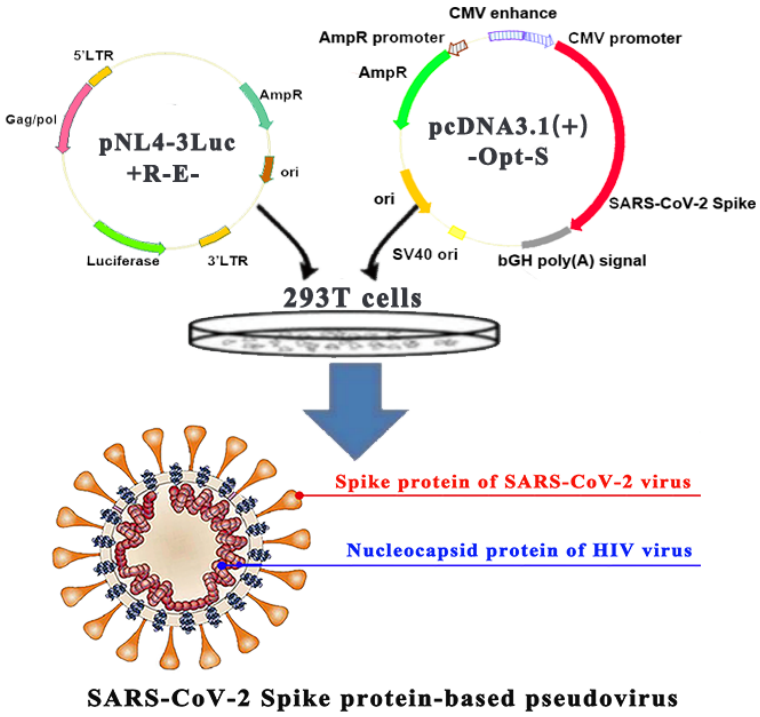

Schematic diagram of the spike protein-containing SARS-CoV-2 pseudovirus.

Exprimental procedures of indentifying the infectiousness of SARS-CoV-2 virus samples based on two-step SERS detections

Anhui Provincial Center for Disease Control and Prevention provided the 1 mL of SARS-CoV-2 with viral load of 10^7 copies/mL. This 1 mL of SARS-CoV-2 was divided into 200 μL, 600 μL, 200 μL, and transferred them to three centrifuge tubes named A, B, and C, respectively. The 600 μL of SARS-CoV-2 in B centrifuge tube was lysed by the lysing process of ultrasound to prepare the lysed SARS-CoV-2 sample. Then, 200 μL of the lysed SARS-CoV-2 was transferred to centrifuge tube C and shaken to mix evenly with the 200 μL of SARS-CoV-2 to prepare the mixture sample of the complete-structure virus and the lysed virus. After the first SERS detection, SARS-CoV-2 with complete viral structure in centrifuge tube A can be identified, and this virus sample exhibits a much severe risk of infectivity. And the infectiousness of the other two virus samples in centrifuge tubes A and B that existing the lysed SARS-CoV-2 cannot be diagnosed at this moment. Therefore, the second Raman detection after RNA elimination and re-lysis was necessary. The TIANSeq RNA Clean Beads was adopted to eliminate SARS-CoV-2 RNA from the lysed SARS-CoV-2 mixture. Firstly, the 200 μL of the lysed SARS-CoV-2 sample and the mixture sample of the complete-structure virus and the lysed virus were transferred into two clean 1.5 mL centrifuge tubes. Then, the magnetic beads binding buffer RM, which has been equilibrated to room temperature, was shaken to mix evenly. And the 440 μL of magnetic beads binding buffer RM was separately transferred to the above-prepared two virus samples and shaken to be mixed evenly. Next, the mixed virus solution was centrifuged to the bottom of the centrifuge tube by the instantaneous centrifugation, and was placed on a magnetic stand for 2-5 min. After the SARS-CoV-2 RNA were completely absorbed by magnetic beads, the upper liquid was carefully aspirated into two other clean 1.5 mL centrifuge tubes. At this moment, the SARS-CoV-2 RNA was eliminated from the upper liquid. Finally, the above-prepared upper liquid was re-lysed by the lysing process of ultrasound. It is worthwhile to note that all experiments on SARS-CoV-2 are required to be carried out in the P2/P3 laboratory.

Supplemental References

1. Yang, L.L., Peng, Y.S., Yang, Y., Liu, J.J., Huang, H.L., Yu, B.H., Zhao, J.M., Lu, Y.L., Huang, Z.R., Li, Z.Y., Lombardi, J.R. (2019). A Novel Ultra-Sensitive Semiconductor SERS Substrate Boosted by the Coupled Resonance Effect. Adv. Sci. *6*, 1900310.
2. Peng, Y.S., Lin, C.L., Long, L., Masaki, T., Tang, M., Yang, L.L., Liu, J.J., Huang, Z.R., Li, Z.Y., Yang, Y. et al. (2021). Charge-Transfer Resonance and Electromagnetic Enhancement Synergistically Enabling MXenes with Excellent SERS Sensitivity for SARS-CoV-2 S Protein Detection. Nano-Micro Lett. *13*, 52.
3. Peng, Y.S., Cai, P. Yang, L.L., Liu, Y.Y., Zhu, L.F., Zhang, Q.Q., Liu, J.J., Huang, Z.R., and Yang, Y. (2020). Theoretical and Experimental Studies of Ti_3C_2 MXene for Surface-Enhanced Raman Spectroscopy-Based Sensing. ACS Omega *5*, 26486−26496.
4. Ye, Y.T., Yi, W.C., Liu, W., Zhou, Y., Bai, H., Li, J.F., Xi, G.C. (2020). Remarkable surface-enhanced Raman scattering of highly crystalline monolayer Ti_3C_2 nanosheets. Sci. China Mater. *63(5)*, 794–805.
5. Islam, S.K., Tamargo, M., Moug, R., and Lombardi, J. R. (2013). Surface-Enhanced Raman Scattering on a Chemically Etched ZnSe Surface. J. Phys. Chem. C *117*, 23372-23377.
6. Wang, X.T., Shi, W.X., Wang, S.X., Zhao, H.W., Lin, J., Yang, Z., Chen, M., Guo, L. (2019). Two-Dimensional Amorphous TiO_2 Nanosheets Enabling High-Efficiency Photoinduced Charge Transfer for Excellent SERS Activity. J. Am. Chem. Soc. *141*, 5856-5862.
7. Cong, S., Yuan, Y.Y., Chen, Z.G., Hou, J.Y., Yang, M., Su, Y.L., Zhang, Y.Y., Li, L., Li, Q.W., Geng, F.X., Zhao, Z.G. (2015). Noble metal-comparable SERS enhancement from semiconducting metal oxides by making oxygen vacancies. Nat. Commun. *6*, 7800.
8. Liu, Q., Jiang, L., and Guo, L. (2014). Precursor-directed self-assembly of porous ZnO nanosheets as high-performance surface-enhanced Raman scattering substrate. Small *10*, 48-51.
9. Wu, H., Wang, H., and Li, G. (2017). Metal oxide semiconductor SERS-active substrates by defect engineering. Analyst *142*, 326-335.
10. Lin, J., Shang, Y., Li, X.X., Yu, J., Wang, X.T., Guo, L. (2017). Ultra-sensitive SERS Detection by Defect Engineering on Single Cu_2O Superstructure Particle. Adv. Mater. *29*, 1604797.
11. Peng, Y.S., Lin, C.L., Tang, M., Yang, L.L., Yang, Y., Liu, J.J., Huang, Z.R., and Li, Z.Y. (2020). Niobium pentoxide ultra-thin nanosheets: A photocatalytic degradation and recyclable surface-enhanced Raman scattering substrate. Appl. Surf. Sci. *509*, 145376.
12. Li, A.R., Lin, J., Huang, Z., Wang, X.T., and Guo, L. (2018). Surface-Enhanced Raman Spectroscopy on Amorphous Semiconducting Rhodium Sulfide Microbowl Substrates. iScience *10*, 1-10.
13. Zhu, Q., Jiang, S.L., Ye, K., Hu, W., Zhang, J.C., Niu, X.Y., Lin, Y.X., Chen, S.M., Song, L., and Luo, Y. (2020). Hydrogen-Doping-Induced Metal-Like Ultra-high Free-Carrier Concentration in Metal-Oxide Material for Giant and Tunable Plasmon Resonance. Adv. Mater. *32*, 2004059.
14. Song, X.Y., Yi, W.C., Li, J.F., Kong, Q.H., Bai, H., and Xi, G.C. (2021). Selective Preparation of Mo_2N and MoN with High Surface Area for Flexible SERS Sensing. Nano Lett. *21*, 4410-4414.
15. Guan, H.M., Yi, W.C., Li, T., Li, Y.H., Li, J.F., Bai, H., and Xi, G.C. (2020). Low temperature synthesis of plasmonic molybdenum nitride nanosheets for surface enhanced Raman scattering. Nat. Commun. *11*, 3889.
16. Wang, K.K., Guo, Z.Y., Li, Y., Guo, Y.X., Liu, H., Zhang, W., Zou, Z.Z., Zhang, Y.L., and Liu, Z.M. (2020). Few-Layer $NbTe_2$ Nanosheets as Substrates for Surface-Enhanced Raman Scattering Analysis. ACS Appl. Nano Mater. *3(11)*, 11363–11371.

17. Quan,Y.N., Yao, J.C., Sun, Y.S., Qu, X., Su, R., Hu, M.Y., Chen, L., Liu, Y., Gao, M., and Yang, J.H. (2021). Enhanced semiconductor charge-transfer resonance: Unprecedented oxygen bidirectional strategy. Sens. Actuators, B *327,* 128903.
18. Aubrey, K.L. and Thomas, G.J. (1992). man spectroscopy of filamentous bacteriophage Ff (fd, M13, f1) incorporating specifically-deuterated alanine and tryptophan side chains. Assignments and structural interpretation. Biophys. J. *60(6),* 1337-1349.
19. Krimm, S. and Bandekar, J. (1986). Vibrational Spectroscopy and Conformation of Peptides, Polypeptides, and Proteins. Adv. Protein Chem. *38,* 181-364.
20. Miura, T. and Thomas, G.J. (1995). Raman Spectroscopy of Proteins and Their Assemblies. Subcell. Biochem. *24,* 55-99.
21. Bandekar, J. (1992). Amide Modes and Protein Conformation. Biochim. Biophys. Acta *1120(2),* 123-143.
22. Cardona, M. (1982). Light Scattering in Solids II, Chapter 2 Resonance Phenomena. (Springer Berlin Heidelberg).
23. Proniewicza, E., Tata, A., Starowicz, M., Wojcik, A., Pacek, J., and Molenda, M. (2021). Is the electrochemical or the "green chemistry" method the optimal method for the synthesis of ZnO nanoparticles for applications to biological material? Characterization and SERS on ZnO. Colloid Surf. A-Physicochem. Eng. Asp. *609,* 125771.
24. Hohenberg, P. and Kohn, W. (1964). Inhomogeneous Electron Gas. Phys. Rev. *136,* B864-B871.
25. Perdew, J.P., Burke, K., and Ernzerhof, M. (1996). Generalized Gradient Approximation Made Simple. Phys. Rev. Lett. *77,* 3865-3868.
26. Monkhorst, H.J. and Pack, J.D. (1976). Special points for Brillouin-zone integrations. Phys. Rev. B *13,* 5188-5192.
27. Ulloa, S., Bravo, C., Ramirez, E., Fasce, R., and Fernandez, J. (2021). Inactivation of SARS-CoV-2 isolates from lineages B.1.1.7 (Alpha), P.1 (Gamma) and B.1.110 by heating and UV irradiation. J. Virol. Methods *295,* 114216.